 ICES-2014-283

Assessment of molecular contamination on the BepiColombo MMO spacecraft

Hiroyuki Ogawa[1]
Institute of Space and Astronautical Science, Sagamihara, Kanagawa, 2525210 JAPAN

Fumitaka Urayama[2]
Space Engineering Development Co.Ltd, Nakano, Tokyo,1640001, JAPAN

Susumu Baba[3] and Eiji Miyazaki[4]
Japan Aerospace Exploration Agency, Tsukuba, Ibaraki, 3058505, JAPAN

Akira Okamoto[5]
NEC Corporation, Fuchu, Tokyo, 1838501, JAPAN

and

Hajime Hayakawa[6]
Institute of Space and Astronautical Science, Sagamihara, Kanagawa, 2525210 JAPAN

The influence of the molecular contaminants (MOC) accumulating on the thermal control surface as well as the optical elements was assessed for the BepiColombo MMO (Mercury Magnetospheric Orbiter). The outgassing and decomposing properties were measured for the dominant outgassing materials according to ASTM-E1559 at low temperatures. The high temperature outgassing property, photo-deposition efficiency and absorption coefficient were obtained by a dedicated experiment. The high temperature evaporation property of deposited MOC was measured using temperature programmed desorption mass spectrometry (TPD-MS). The simulation of the MOC transport was conducted to predict the MOC thickness and the increase in the solar absorptivity on the MMO surface. The temperature prediction taken the degradation of thermo-optical property into account is also shown.

Nomenclature

$\dot{M}_i$	=	outgas rate of the source material *i*, [g g^{-1} sec^{-1}]
a_i, b_i	=	outgas rate constant of the source material *i*
t	=	elapsed time, [sec]
$s_{UV,i}$	=	photodeposition efficiency of the molecules from the source material *i*
χ_i	=	thickness of the deposited material from the source material *i*, [cm]
ρ	=	density of the deposited material, [g cm^{-3}]
Φ_i	=	mass fluence of the molecules from the source material *i*, [g cm^{-2}]
$\tau_i(\lambda)$	=	spectral transmittance of the contaminated substrate by the molecules from the source material *i*
$\tau_0(\lambda)$	=	spectral transmittance of the virgin substrate
λ	=	wavelength, [nm]

[1] Manager, Thermal Systems and Fluid Dynamics Group, 3-1-1 Yoshinodai, Chuo, Sagamihara.
[2] Manager, Spacecraft Engineering Group, 5-62-1 Nakano, Nakano, Tokyo.
[3] Engineer, Electronic Devices and Materials Group, 2-1-1 Sengen, Tsukuba.
[4] Associate Senior Engineer, Electronic Devices and Materials Group, 2-1-1 Sengen, Tsukuba.
[5] Senior Manager, Space Systems Division, 1-10 Nisshincho, Fuchu, Tokyo.
[6] Project Manager, BepiColombo project, 3-1-1 Yoshinodai, Chuo, Sagamihara.

$\alpha_{MOC,i}(\lambda)$ = spectral optical absorptance of the deposited material from the source material *i*, [cm^{-1}]
α_i = solar absorptance of the deposited second surface mirror by the molecules from the source material *i*
$\rho_0(\lambda)$ = spectral reflectance of the virgin second surface mirror
$S(\lambda)$ = spectral solar intensity, [W m^{-2} nm^{-1}]
$\dot{M}_{u,i}(t, T_s)$ = outgas rate per unit mass at time *t* at temperature T_s, [g g^{-1} sec^{-1}]
a_i', b_i' = outgas rate constant of the source material *i*
T_s = temperature of the source, [K]
E_s = activation energy of the source material *i*, [J mol^{-1}]
R = universal gas constant, [J K^{-1} mol^{-1}]
$k_{2,i}$ = evaporation rate constant of the deposited molecules from the source material *i*, [sec^{-1}]
$A_{evap,i}$ = frequency factor of the deposited molecules from the source material *i*, [sec^{-1}]
$E_{evap,i}$ = desorption energy of the deposited molecules from the source material *i*, [J mol^{-1}]
$(k_3 q)_i$ = effective photochemical cross section of the molecules from the source material *i*, [cm^{-2}]
I = number of photons per unit area per unit time, [cm^{-2} sec^{-1}]

MOC = Molecular Contaminants
TPD-MS = Temperature Programmed Desorption Mass Spectroscopy
MMO = Mercury Magnetospheric Orbiter
MPO = Mercury Planetary Orbiter
MOSIF = Magnetospheric Orbiter Sunshade and Interface
MTM = Mercury Transfer Module
MCS = Mercury Composite Spacecraft, composed of MMO, MOSIF, MPO and MTM
SSM = Second Surface Mirror
MLI = Multi Layer Insulation
HGA = High Gain Antenna
ADM = Antenna Despun Motor
APM = Antenna Pointing Mechanism
MGA = Medium Gain Antenna, (TX: Transmitter, RX: Receiver)
UV, VUV = Ultra-violet, Vacuum Ultra-violet
SSC = Star Scanner
MSASI = Mercury's Sodium Atmosphere Spectral Imager
CVCM = Collected Volatile Condensable Materials
TQCM = Thermoelectric Quartz Crystal Microbalance
MTA = Mercury True Anomaly
EOL = End of Life

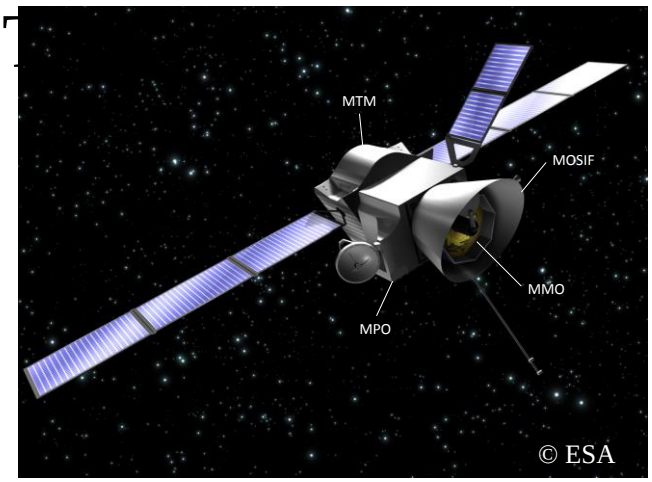

Figure 1. Mercury Composite Spacecraft.

I. Introduction

HE BepiColombo mission to Mercury is the ESA's Fifth Cornerstone Mission, and a joint mission between ESA and the Japan Aerospace Exploration Agency (JAXA), executed under ESA leadership. The mission comprised of two science elements that are the Mercury Planetary Orbiter (MPO) and the Mercury Magnetospheric Orbiter (MMO). The system baseline is the launch of the Mercury Composite Spacecraft (MCS: Figure 1) on an Ariane 5 during the launch window in 2016. The MCS is composed of MMO, MOSIF (Magnetospheric Orbiter Sunshade and Interface), MPO, and the MTM (Mercury Transfer Module). The MOSIF provides a sun-shield for MMO to be protected from the strong sun illumination until MMO separation. The MTM is utilized during the interplanetary cruise. JAXA (Japan Aerospace Exploration Agency) provides the MMO, and ESA provides the launch, MOSIF, MPO and the

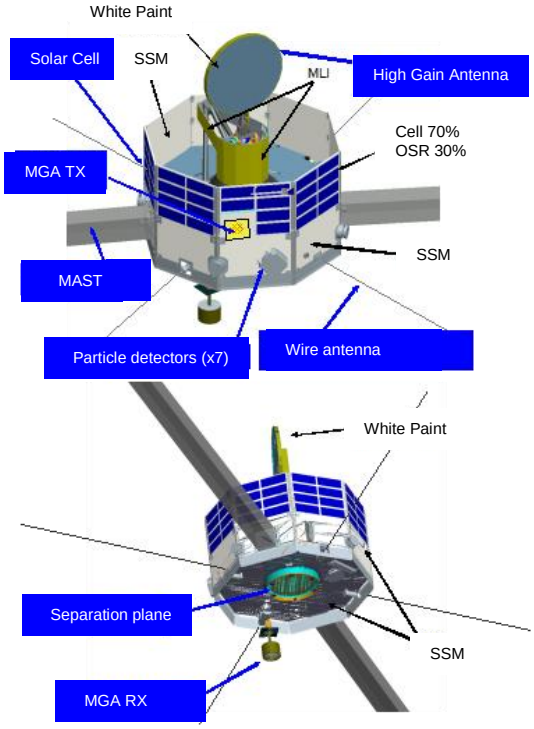

Figure 2. MMO spacecraft.

MTM.

The MMO is a spin-stabilized spacecraft, and its spin axis is pointed nearly perpendicular to the Mercury revolution plane. The harsh environment near Mercury (0.31AU from the Sun at perihelion) imposes 11 solar constant irradiation on the MMO spacecraft, while its thermal control system is required to maintain the onboard equipment and the spacecraft structure in a proper temperature range during the entire mission phases. The MMO is controlled by means of passive thermal design techniques and some components are controlled by means of a combination of passive and active techniques. The passive thermal control elements are Second Surface Mirror (SSM), the thermal shield, paints, films, and Multi-Layer-Insulation blankets (MLI). All external surfaces should be electrical conductive due to scientific requirements. The details of the thermal control system of MMO are presented in [1]-[3].

The MMO has an octagonal shape, which can be surrounded by a 1.8 m diameter circle (Figure 2). The height of the side panel is 1.06m. The instruments are located on the upper and lower decks with 0.4m in between them. The HGA (High Gain Antenna) is a helical array antenna of 0.8m diameter. The HGA is pointed towards the Earth by the ADM (Antenna Despun Motor) and an elevation control mechanism APM (Antenna Pointing Mechanism). ADM and APM are protected from direct solar illumination by the 'APM sunshade,' which is made of MLI. The MGA (Medium Gain Antenna) RX (Receiver), a bi-reflector type antenna, is mounted on the lower surface with an extensible mechanism. Most of the scientific instruments (particle sensors, etc.) are allocated on the lower deck and look out of the side panels through cut-outs, while two pairs of probe antennas for plasma wave instruments and one pair of extensible booms for magnetometers are installed on the outside. The scientific instruments looking out of side panels are covered by a dedicated sun-shield to prevent direct solar heat input as much as possible. The extendible booms for magnetometers are covered by a single-layer Germanium-coated Black Kapton to avoid direct solar illumination to the MMO interior through the cut-outs for the booms.

MCS will be launched in 2016, and will perform a first swing-by towards the inner solar system at Earth. Then the perihelion will be lowered to cross the Mercury orbit by two swing-bys at Venus. MCS will be slowed down by four additional Mercy swing-bys to a low relative velocity, which allows weak stability boundary capture into a highly elliptic orbit around Mercury. With the separation of the MTM the Mercury approach phase begins, which covers capture at Mercury and orbit insertion maneuvers to reach the final orbits of MMO and MPO. MMO is protected against sunlight by the MOSIF until ejection into its final orbit.

Since MMO is exposed to the harsh environment and MMO becomes much higher in temperature, more outgassing will occur than with conventional satellites around Earth. Molecular contamination (MOC) of the MMO surface is expected to be enhanced due to the larger amount of outgas and the higher intensity of sunlight, especially vacuum ultra-violet (VUV). MOC causes the degradation of thermo-optical properties of the thermal control surfaces as well as the sensor performance such as a star scanner (SSC) and the Mercury's sodium atmosphere spectral imager (MSASI).

This paper describes the assessment of molecular contamination on the MMO spacecraft.

II. MOC Source Materials

The main source materials of MOC which release the majority of outgas were selected according to the CVCMs (collected volatile condensable materials) and weights of the materials used in MMO. We selected four main source materials; an epoxy adhesive Hysol® EA9396, a silicone adhesive RTV-S691, a silicone adhesive ELASTOSIL®-S692, and a silicone transfer adhesive TRANS-SIL®. Hysol® EA9396 is used in the solar cell panels. RTV-S691 is

used to bond solar-cells and as the thermal filler. ELASTOSIL®-S692 is used to bond SSMs. TRANS-SIL® is used in MLI and the extensible booms.

III. MOC Accumulation until Separation

The thermal environment of MMO is different before and after the separation from MOSIF: The MMO is low in temperature and not illuminated by sunlight before the separation, while it is high in temperature and illuminated after the separation. Since the outgassing characteristics depend on temperature and the MOC accumulation rates depend on temperature and the intensity of sunlight, we treat the MOC accumulation problem differently.

We modelled the outgas rate (g g^{-1} s^{-1}) of the source material *i* as:

$$\dot{M}_i = {}^{a_i}/_{t^{b_i}} \qquad (1)$$

where t is the time after the launch. The outgas rate constants a_i and b_i depend on the material. They were obtained by experiments according to ASTM-E1559 [4]. The source temperature was 303K, while the TQCM (Thermoelectric Quartz Crystal Microbalance) temperatures were 143K, 193K, and 253K, in the experiments. The outgas rate constants were obtained by the measured data of the TQCM of 143K.

The sticking coefficients, the ratio of the accumulating mass per unit time per unit area to the incoming mass flux to a unit surface (g cm^{-2} s^{-1}), were obtained from the TQCM data for 193K and 253K, assuming the sticking coefficient for the 143K surface is 1.0.

The MOC accumulation on the MMO surface until the separation was calculated using the J-SPICE software [5]. J-SPICE calculates the mass transfer from the source surface to the target surface using the ray-trace and the Monte-Carlo techniques. J-SPICE considers the direct flux and the flux re-emitted from spacecraft surfaces, while does not take the self-scattering and the ambient scattering of the contaminant molecules into account since the gas density around MMO is low enough. Although the outgas rate depends on the temperature, we assumed it was constant at 303K. Since the sticking coefficient is larger for lower temperature, we selected the surface temperature from 143K, 193K and 253K as it is lower and closest to the analyzed MMO temperature, in the J-SPICE mass transfer analysis. Furthermore the MMO temperature used in the temperature selection was that analyzed for the case of 0.3 AU (Astronomical Unit) from the Sun, although it is unrealistically worst case for the MOC analysis. Figure 3 shows the assumed temperature distribution. The MMO temperature is lower than 303K (30°C). The accumulated mass on each surface before separation was calculated by integrating over 6 years, which is long enough for the cruise phase analysis. Figure 4 shows the analysis results.

The dominant material is ELASTOSIL®-S692. The MOC accumulation is large on the side panel, while it is small on the lower deck (~10^{-7} g/cm^2). The MOC level on the lower deck is not risky for the SSC and MSASI.

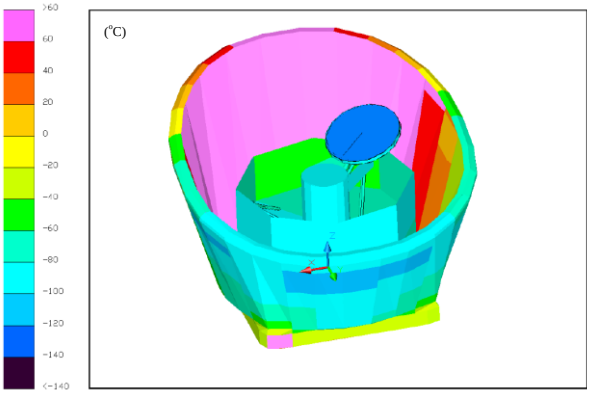

Figure 3. MMO Temperature before separation.

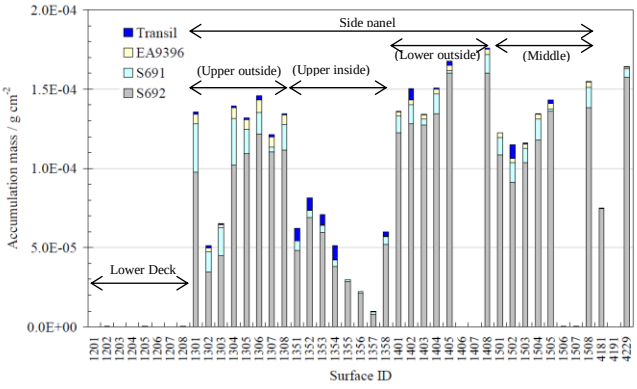

Figure 4. MOC accumulation on MMO surface.

IV. MOC Evaporation at Separation

At the separation MMO is illuminated and heated up by sunlight. The increase in temperature will evaporate the accumulated MOC, while the UV in sunlight will bond the MOC and increase the solar absorptance by the photo-deposition effect. To find out what will occur at the separation we conducted dedicated experiments: The MOC deposited SSM was exposed to UV light. SSMs of 25 ^{o}C were exposed to the outgas flow from each source material (Hysol® EA9396, RTV-S691, ELASTOSIL®-S692, and TRANS-SIL®) of 125^{o}C in vacuum. Then, the MOC deposited SSMs were exposed to 10 solar constant UV light made by 5kW Xe short-arc lamp. The SSM masses as well as thermo-optical properties (solar absorptance and infra-red emissivity) were measured before and after the MOC deposition, and after UV illumination. Although MOCs were deposited in layers of 5nm, 100nm, 100nm, and 120nm on SSMs for Hysol® EA9396, RTV-S691, ELASTOSIL®-S692, and TRANS-SIL®, respectively, before UV illumination, the MOC disappeared after UV illumination: The SSM masses decreased and the thermo-optical properties came back to those before the MOC deposition. Since the SSM temperature was 80^{o}C due to the UV illumination, the MOC evaporated by the temperature increase before it is photo-chemically bonded on the SSM. Therefore, it is shown that the MOC accumulated during the cruise phase will disappear at the separation from MOSIF.

V. MOC Accumulation and Degradation of Solar Absorptance

A. Experiments

We conducted dedicated experiments to estimate the outgas rates of the source materials and the MOC deposit rates on the surface in the Mercury environment; high temperature and VUV illuminated. Figure 5 shows the apparatus of the dedicated experiments. The apparatus was located in the thermal vacuum chamber, whose inner walls are cooled to -200^{o}C by liquid nitrogen. The source material (adhesive) in the effusion cell (Figure 6) was heated above 160^{o}C. The source adhesive was sandwiched by 4cm x 4cm Aluminum plates to simulate the outgas rate from the narrow opening of the adhesive. The outgas molecules impinge to the TQCM (Figure 7) and a CaF_2 plate passing through an orifice (3mm diameter, 3mm thickness) drilled on the effusion cell wall. The TQCM measured the fluence of the outgas molecules; the TQCM temperature was -10^{o}C. The CaF_2 plate was illuminated by a VUV lamp, and the plate temperature was controlled above 130^{o}C. The VUV lamp was kept in the lamp house to prevent the CaF_2 plate from contamination from the VUV lamp itself: The VUV light was beamed out through an MgF_2 window of the lamp house. The experimental conditions are shown in Table. 1. The effusion cell temperature and the CaF_2 plate temperature were chosen according to the thermal analyses of the MMO in the Mercury orbit. The VUV intensity was equivalent to 0.1 ~ 1 solar constant. Although the VUV illuminated time and the VUV intensity were limited by the availability of the thermal vacuum chamber and the VUV lamp used, respectively, comparing the actual Mercury environment, the supporting analysis described in the subsequent subsections enables

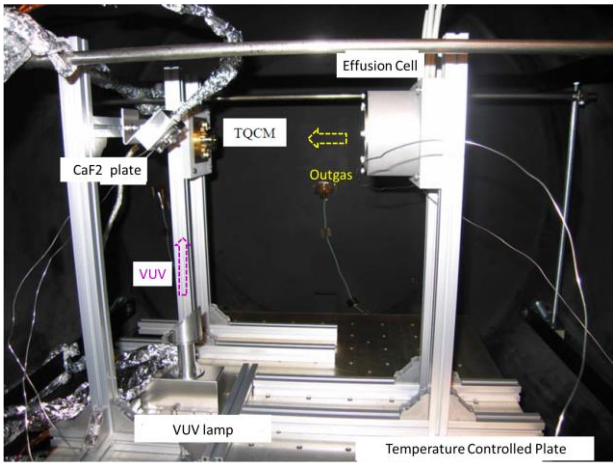

Figure 5. Apparatus of Outgas and MOC Photodeposition Experiment.

Table 1. Experimental condition

Material	RTV-S691	ELASTOSIL ®S692	TRANS®-SIL
Effusion Cell Temperature	230°C	1) 230°C 2) 226°C 3) 184°C 4) 165°C	240°C
CaF_2 Plate Temperature	144°C	1) 143°C 2) 163°C 3) 129°C 4) 165°C	173°C
VUV Illuminated Time	72 hours	1) 57 hours 2) 64 hours 3) 66 hours 4) 69 hours	58 hours

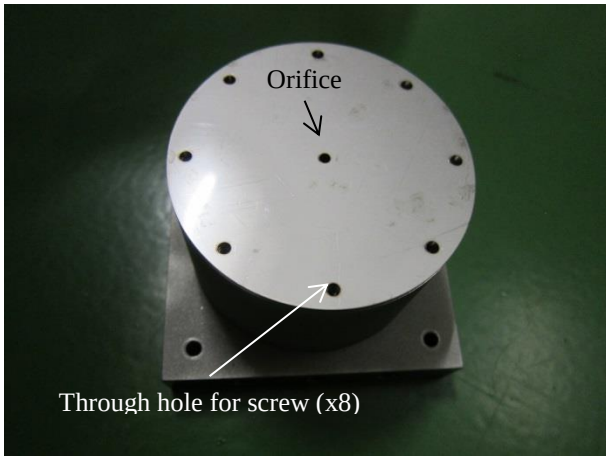

Figure 6. Effusion Cell.

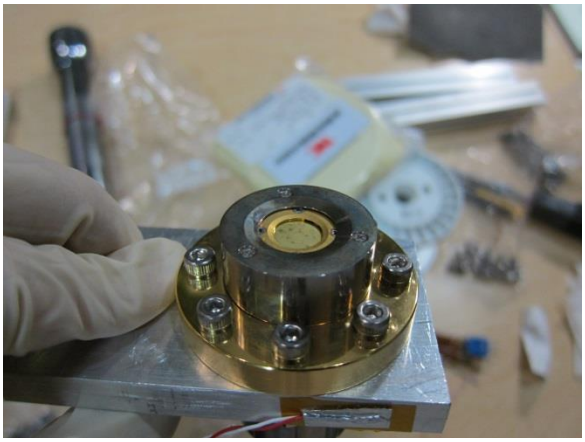

Figure 7. TQCM.

us the prediction of the MOC deposition and the resulting increase in the solar absorptance. Note that Hysol® EA9396 was not taken into consideration in the experiment as well as in the subsequent analysis, since (1) Hysol® EA9396 is an epoxy adhesive and therefore the MOC from it hardly photodeposit on a surface, and (2) the amount of MOC deposit is much smaller compared to that from other adhesives.

After the experiment, the CaF_2 plate was analyzed: we measured (1) the spectral transmittance of the MOC, $\tau(\lambda)$, using a UV/VIS/NIR spectrophotometer and an FT-IR spectrophotometer, and (2) the thickness of the MOC, χ, using an X-ray photoelectron spectroscopy.

The photodeposition efficiency of MOC from adhesive *i*, $s_{UV,i}$ is the ratio of the deposited mass to the impinged mass:

$$s_{UV,i} = \frac{\chi_i \cdot \rho}{\Phi_i} \tag{2}$$

Where χ_i is the MOC thickness from adhesive *i* [cm], ρ is the density of MOC (assumed 1 [g/cm^3]), and Φ_i is the MOC flux [g cm^{-2}] to the CaF_2 plate. The MOC flux is calculated from the TQCM data.

The spectral optical absorptance of MOC, $\alpha_{MOC,i}$ is obtained from:

$$\tau_i(\lambda) = \tau_0(\lambda) \cdot exp\left(-\alpha_{MOC,i}(\lambda) \cdot \chi_i\right) \tag{3}$$

Here $\tau_i(\lambda)$ and $\tau_0(\lambda)$ are the spectral transmittance at the wavelength λ for the CaF_2 plate deposited by the MOC from the adhesive *i* and the spectral transmittance at the wavelength λ for the 'virgin' CaF_2 plate, respectively. The solar absorptance of MOC deposited SSM, α_i, is:

$$\alpha_i = \frac{\int\left[1-\rho_0(\lambda)\cdot exp\left(-2\alpha_{MOC,i}(\lambda)\cdot\chi_i\right)\right]\cdot S(\lambda)d\lambda}{\int S(\lambda)d\lambda} \tag{4}$$

Where $\rho_0(\lambda)$ is the spectral reflectance of the `virgin' SSM at the wavelength λ, and $S(\lambda)$ is the spectral solar intensity.

The outgas rate per unit mass of the adhesive *i*, at time *t*, $\dot{M}_{u,i}(t, T_s)$ [g g^{-1} s^{-1}], is obtained from the TQCM data, with taking the effusion cell temperature time history into account:

$$\dot{M}_{u,i}(t, T_s) = \frac{a_i'}{t^{b_i'}} \cdot exp\left(-\frac{E_{s,i}}{RT_s}\right) \tag{5}$$

Here a_i' and b_i' are the constants for the adhesive *i*, T_s is the absolute temperature of the MOC source, $E_{s,i}$ is the activation energy [J mol^{-1}], and R is the universal gas constant [J K^{-1} mol^{-1}].

B. Temperature Programmed Desorption Mass Spectrometry

To obtain the evaporation property of deposited MOC on a surface, we measured the temperature dependence of evaporation rate of deposited MOC and molecular mass of evaporated gas using temperature programmed desorption mass spectrometry (TPD-MS). The SSM sample, on which the outgassing contaminants from (1) RTV-S691, (2) ELASTOSIL®-S692 and TRANS®-SIL of 230°C were deposited, was gradually heated at the rate of 10°C/min up to 500°C.

The evaporation rate constant ($k_{2,i}$) of the adhesive, i, is obtained from the TPD-MS measured data:

$$k_{2,i} = A_{evap,i} \cdot exp\left(-\frac{E_{evap,i}}{R \cdot T}\right) \quad (6)$$

Where $A_{evap,i}$ is the frequency factor, $E_{evap,i}$ is the desorption energy, R is the universal gas constant, and T is the absolute temperature, for the adhesive i. The effective photochemical cross section of the MOC from the adhesive i, $(k_3 q)_i$ is;

$$(k_3 q)_i \approx \frac{s_{UV,i} \cdot k_{2,i}}{(1 - s_{UV,i}) \cdot I} \quad (7)$$

Here I is the number of photons impinging on the CaF_2 surface per unit area per unit time [cm^{-2} s^{-1}], which is calculated by the catalogue data and the transmissivity measurement of MgF_2.

C. Experimental results

Figures 8 and 9 show the photodeposition efficiencies and the effective photochemical cross sections, respectively. In Figure 9 the photochemical cross section of DC704 (tetramechyl-tetraphenil-trisiloxane) obtained by Stewart *et.al*. is added for comparison. The photochemical cross section of the 4th experiment of ELASTOSIL®-S692 is larger than those of the 1st to 3rd experiments. The reason for it is considered the difference of VUV intensity: The CaF_2 plates were placed in the weaker VUV illuminated region in the 1st to 3rd experiments.

Figures 10 and 11 show the absorption coefficients and the solar absorptances, respectively. In Figure 11 the experimental results of Mossan *et.al* as well as that of DC704.

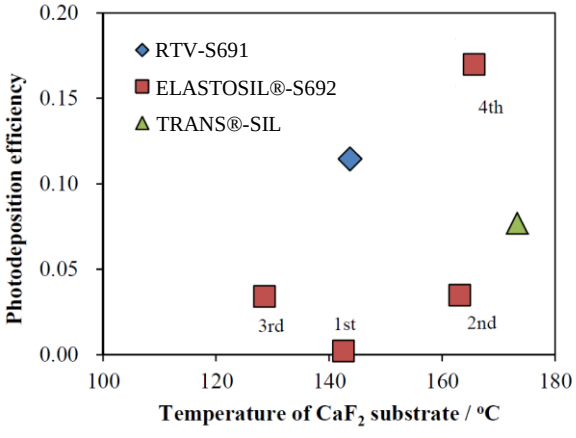

Figure 8. Photodeposition Efficiency.

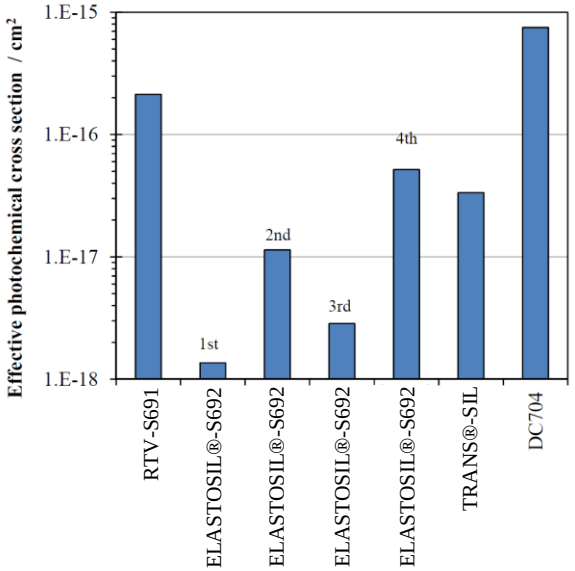

Figure 9. Effective Photochemical cross section. *DC704 data is from [6].*

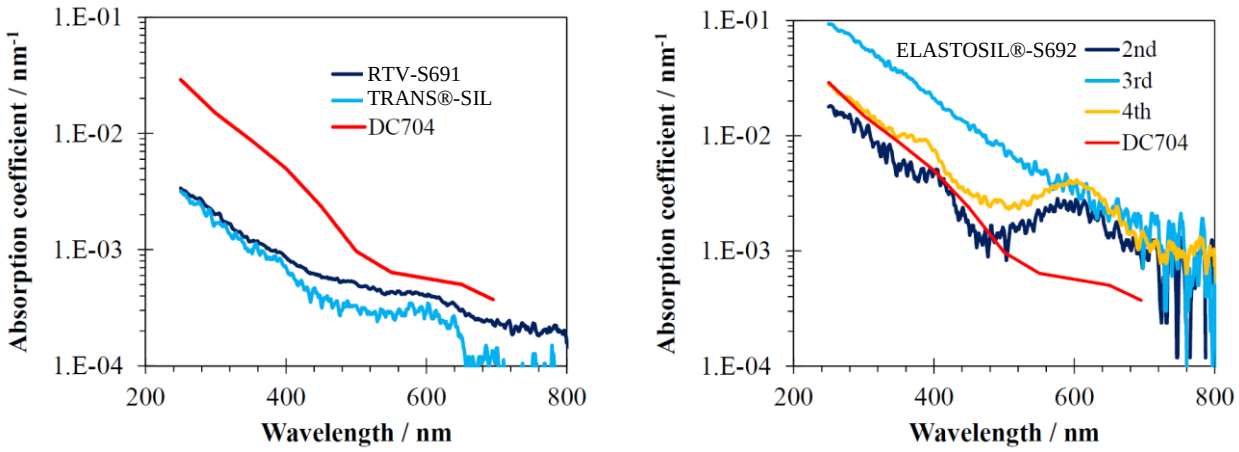

Figure 10. Absorption coefficient. *DC704 data is from [6].*

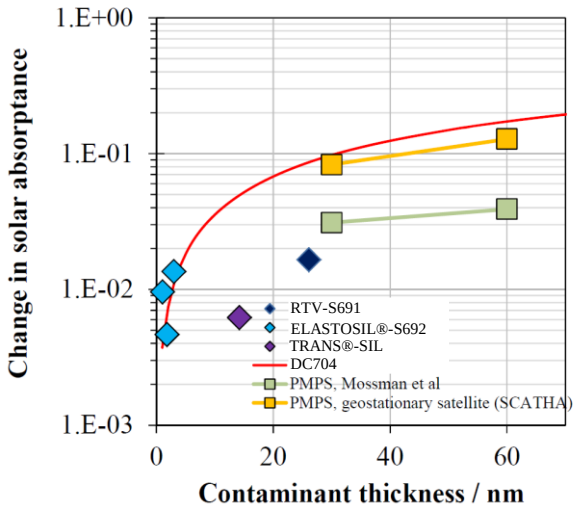

Figure 11. Absorption coefficient. *DC704 and PMPS data is from[6] and [7], respectively.*

D. Change in solar absorptance of MMO surface in orbit

The MOC deposition on the MMO surface in the scientific observation orbit after the separation was calculated using the J-SPICE software [5], which takes into account the geometry of MMO, the material constituting the MMO surfaces, and the temperature of the surfaces, and assumes that the self-scattering and the ambient scattering of the contaminant molecules do not occur. We took the MMO temperature profile into account, which depends not only on the position in the Mercury orbit but also on the Mercury position; the Mercury True Anomaly (MTA). The outgas rate was calculated by Eq. (5). Note that for the initial outgas rate was assumed that the side panels of MMO are baked out at 180°C for 10 days. The MOC deposition rate on the MMO surface was computed from Eqs. (2), (6), and (7). After the J-SPICE analysis we obtained the MOC deposited thickness, and then the change in the solar absorptance by Eq. (4). Figure 12 shows the change in the solar absorptance of the MMO surface after 2 years in the Mercury orbit. The degradation of the solar absorptance is most severe near the booms, where the outgas molecules are reflected back by the booms.

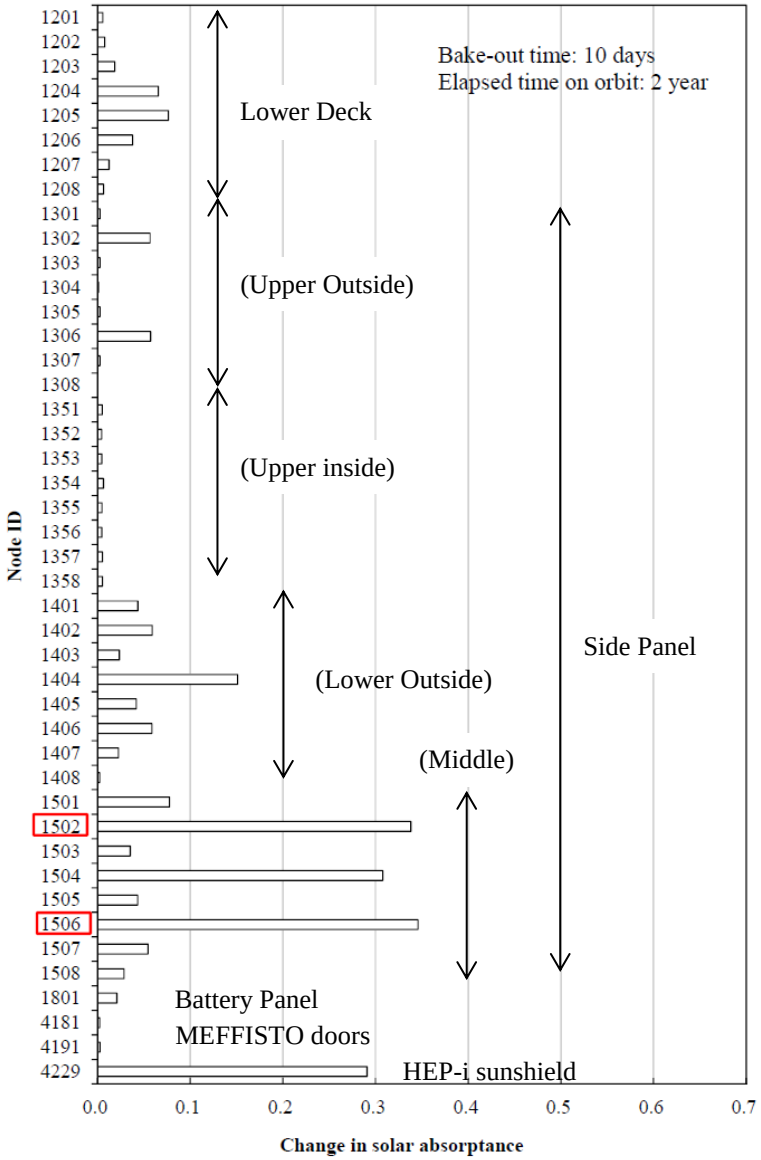

Figure 12. Change in solar absorptance after 2 years in Mercury orbit.

E. Influence on MMO temperature

The surface areas of the solar absorptance obtained in the section D exceed the previously assumed EOL values: 0.3 for SSMs. The previous EOL value of the SSM solar absorptance was obtained 0.3 by adding the extrapolation of the 11 years degradation flight data of the Solar and Heliospheric Observatory Spacecraft (SOHO) at the L1 libration point and the margin of 0.1. The flight data includes the space environmental effects of the MOC from the spacecraft, and the 11 years UV and charged particles irradiations. Although the UV and charged particles irradiations in case of SOHO are considered to be equivalent to those in case of MMO, the MOC influence is different. The thermal analysis, therefore, was conducted in order to assess the influence of MOC. In the analysis the solar absorptance of the surface was assumed the sum of the EOL value (e.g. SSM is 0.3) and the solar absorptance change due to MOC, shown in Figure 12. Table 2 shows the result.

The instrument temperatures inside MMO increase by 2°C to 5°C due to MOC, and they are still in the allowable range. The side panel temperature, however, exceeds the upper limit of 230°C. We qualified the side panels at 245

°C +/- 10°C. Therefore we consider the risk is low. Although HGA increases in temperature by 80 – 100 °C, and the APM RJ temperature increases by 20°C because it connects with HGA via thermal insulation, the temperatures are still in the allowable range. Note that it is not a problem that MEFFISTO exceeds the upper temperature limit of 80°C.

Table 2. MMO temperature increase due to MOC.

Orbit HOT Case 0.3AU	Allowable Temperature		BASE		CASE-4		⊿T CASE-4—BASE	
Node Definition	max	min	max	min	max	min	max	min
MMO Upper Deck			62.5	21.9	63.4	23.2	0.9	1.3
MMO Lower Deck			58.1	-18.0	60.3	-16.3	2.2	1.7
Battery Panel			39.0	-6.6	38.9	-5.8	-0.1	0.8
Solar Cell	230	-200	*227.5*	-76.5	**241.1**	-76.1	13.6	0.4
Solar Cell Average	230	-200	217.4	-69.2	219.6	-68.7	2.3	0.4
Upper Prism Outer	230	-200	*226.6*	-76.5	**236.2**	-76.1	9.5	0.4
Upper Prism Inner	230	-200	**221.5**	-76.3	**230.2**	-75.9	8.7	0.4
Side Prism Outer	230	-200	217.2	-66.7	**245.3**	-66.2	28.1	0.5
Side Prism Inner	230	-200	216.4	-66.5	**243.3**	-66.0	26.9	0.5
Lower Prism Outer(with Fin)	230	-200	**221.0**	-60.2	**233.2**	-59.5	12.2	0.7
Lower Prism Inner(with Fin)	230	-200	**221.2**	-60.1	**233.2**	-59.4	12.1	0.7
Thrust Tube			47.5	4.0	48.9	5.2	1.4	1.2
Bulkhead			60.1	5.4	61.0	6.6	1.0	1.3
Thrust Tube Ring			43.8	3.1	45.0	4.3	1.2	1.2
HGA (REF)	400	-200	222.8	-2.7	242.2	0.6	19.3	3.3
HGA (Back MLI)			225.9	-117.9	291.0	-113.2	65.2	4.7
ADM Pedestal			70.4	25.1	68.4	26.3	-2.0	1.3
Upper Deck MLI	290	-200	191.8	-103.0	198.1	-102.3	6.3	0.7
Side Prism Inner MLI	290	-200	115.5	-4.4	117.7	-2.6	2.2	1.8
MGA Case			238.1	-42.9	239.4	-42.9	1.3	0.0
MGA Horn			203.6	137.4	202.9	137.0	-0.7	-0.4
MGA Parabola			177.2	-18.1	177.7	-18.0	0.4	0.1
APM Sunshade MLI	290	-200	275.8	-118.2	273.2	-118.3	-2.6	-0.1
ADM Pedestal Outer MLI(out side)	290	-200	165.8	-113.5	163.9	-113.3	-1.9	0.2
ADM Pedestal Inner MLI			54.5	26.9	53.8	27.7	-0.7	0.9
GN2 TANK	60	-30	44.3	23.3	44.6	24.2	0.4	0.9
ADM SRH Pedestal IF	80	-20	**62.4**	**55.1**	**61.3**	**54.2**	**-1.1**	**-0.8**
APM SSCOV	130	-35	**88.0**	**68.9**	**90.3**	**71.5**	**2.3**	**2.7**
APM CASE2	120	-30	**85.1**	**67.1**	**86.6**	**68.8**	**1.5**	**1.8**
APM CLC_A	121	-184	**87.9**	**68.3**	**89.8**	**70.7**	**2.0**	**2.3**
APM RJ(TEMP)	150	-30	**112.1**	**82.8**	**132.0**	**95.8**	**19.9**	**13.0**
APM RJ(TEMP)	150	-30	**86.4**	**67.3**	**90.2**	**71.5**	**3.8**	**4.2**
APM MOT	150	-30	**88.3**	**68.2**	**87.2**	**67.3**	**-1.1**	**-0.9**
APR	65	-30	**52.8**	**33.0**	**54.5**	**34.7**	**1.7**	**1.7**
BAT	30	0	**15.1**	**5.0**	**15.4**	*5.0*	**0.4**	**0.0**
DMC	60	-30	**47.3**	**22.5**	**48.4**	**23.6**	**1.1**	**1.2**
DRU	55	-30	**43.0**	**14.3**	**44.6**	**16.0**	**1.6**	**1.7**
XTRP-A	63	-30	**50.7**	**19.5**	**52.7**	**21.4**	**2.0**	**1.9**
ENA MAIN	70	-35	**44.2**	**11.6**	**46.5**	**13.7**	**2.3**	**2.2**
HEP-ele Case(TRP)	80	-30	**44.6**	**14.4**	**46.3**	**16.2**	**1.7**	**1.7**
HEP-ion Case(TRP)	80	-30	**49.7**	**18.0**	**51.8**	**19.9**	**2.1**	**1.9**
MDP	65	-30	**42.0**	**7.5**	**43.0**	**8.8**	**1.1**	**1.3**
MEA1 Preamp/HV Housing(TRP)	85	-40	**42.9**	**6.0**	**47.3**	**10.1**	**4.4**	**4.1**
MEA2 Preamp/HV Housing(TRP)	85	-40	**48.7**	**13.6**	**50.8**	**15.6**	**2.1**	**2.0**
MEFISTO-S1 Body	80	-50	**84.0**	**43.2**	**84.8**	**44.1**	**0.9**	**0.9**
MEFISTO-S2 Body	80	-50	**83.7**	**44.2**	**84.2**	**44.8**	**0.5**	**0.6**
MGF CAN1 -Z(TRP)	100	-30	**46.2**	**35.3**	**50.3**	**39.2**	**4.0**	**4.0**
MIA Case(TRP)	85	-40	**53.6**	**26.3**	**56.7**	**29.3**	**3.2**	**2.9**
MSA SENSOR BASE	90	-40	**42.7**	**14.7**	**44.8**	**16.8**	**2.1**	**2.0**
MSASI BASE PLATE(TRP)	60	-10	**40.5**	**12.9**	**41.6**	**14.0**	**1.1**	**1.1**
SC CAN1-Z(TRP)	100	-30	**52.5**	**39.7**	**56.9**	**43.9**	**4.4**	**4.2**
WPT1 BASE-PLT(TRP)	120	-180	**87.8**	**51.4**	**89.3**	**53.0**	**1.5**	**1.5**
WPT2 BASE-PLT(TRP)	120	-180	**77.7**	**41.5**	**79.3**	**43.2**	**1.7**	**1.7**
HGA LIB			**226.5**	**54.4**	**318.3**	**66.3**	**91.8**	**11.9**
HGA WG			**227.5**	**56.0**	**307.8**	**67.3**	**80.3**	**11.3**
HGA MLI			**202.7**	**-98.5**	**311.1**	**-88.9**	**108.3**	**9.6**

Internal instruments

Internal instruments

VI. Conclusion

The MOC influence on the MMO thermal control system was assessed. The experiments were conducted to produce the data required for the outgas analysis. The degradation due to MOC was estimated. The thermal analysis was conducted with the previously assumed EOL value of the solar absorptance plus the estimated degradation due to MOC. Note that its assumption is the worst case of the worst because the previously assumed EOL value also includes some influence of MOC. The analyzed temperatures were in the allowable range except the side panels. The side panel temperature did not exceed the qualification temperature: The side panel temperature increase is considered a low risk.

References

[1]Ogawa, H., Yamazaki, T., Okamoto, A., Miyazaki, S., Ohnuki, H., Fukuyoshi, F., Iwata, N., "BepiColombo/MMO Thermal Control System," *40th International Conference on Environmental Systems (ICES2010)* [Online Proceedings], AIAA, Reston, VA, 2010.

[2]Ogawa, H., Yamazaki, T., Okamoto, A., Iwata, N., Okazaki, S., Irikado, T., Fukuyoshi, F., "BepiColombo/MMO Thermal Test Model Testing," *41th International Conference on Environmental Systems (ICES2011)* [Online Proceedings], AIAA, Reston, VA, 2011.

[3]Ogawa, H., Yamazaki, T., Okamoto, A., Iwata, N., Okazaki, "BepiColombo Mercury Magnetospheric Orbiter Flight Model Thermal Analysis," *42th International Conference on Environmental Systems (ICES2012)* [Online Proceedings], AIAA, Reston, VA, 2012.

[4]ASTM E1559-00, Standard Test Method for Contamination Outgassing Characteristics of Spacecraft Materials, 2001.

[5]Hayashi, T., Urayama, F., Takeda, N., Baba, N, "Modeling of Material Outgassing and Deposition Phenomena," *Proc. of SPIE*, Vol. 5526, pp.137-146, 2004.

[6]Arnold, G.S., Luey, K., "Photochemically Deposited Contaminant Film Effects," *Proc. of SPIE*, Vol. 2864, pp.269-285, 1996.

[7]Mossman, D.L., Bostic, H.D., Carlos, J.R., "Contamination Induced Degradation of Optical Solar Reflectors in Geosynchronous Orbit," *Proc. of SPIE*, Vol. 777, pp.12-19, 1987.